Spatial Extent of New Particle Formation Events over the Mediterranean basin from multiple ground-based and airborne measurements

Kevin Berland[1], Clémence Rose[1], Jorge Pey[2], Anais Culot[1], Evelyn Freney[1], Nikolaos Kalivitis[3], Giorgios Kouvarakis[3], José Carlos Cerro[4], Marc Mallet[8], Karine Sartelet[6], Matthias Beckmann[7], Thierry Bourriane[8], Greg Roberts[8], Nicolas Marchand[2] Nikolaos Mihalopoulos[3,9] and Karine Sellegri[1]

[1]Laboratoire de Météorologie Physique, CNRS UMR 6016, Université Blaise Pascal, Aubière, France

[2]Aix-Marseille Université, CNRS, LCE, UMR 7376, 13331, Marseille, France

[3]Environmental Chemical Processes Laboratory, University of Crete, Heraklion, Crete, 71003, Greece

[4]Laboratory of Environmental Analytical Chemistry, Illes Balears University, Palma, 07122, Spain

[5]Laboratoire d'Aérologie (LA), Université de Toulouse, CNRS, Toulouse, France

[6]CEREA, joint laboratory Ecole des Ponts ParisTech - EDF R&D, Université Paris-Est, 77455 Champs sur Marne, France.

[7]Laboratoire Interuniversitaire des Systèmes Atmosphériques (LISA), UMR-CNRS 7583, Université Paris-Est-Créteil (UPEC) et Université Paris Diderot (UPD), Institut Pierre Simon Laplace (IPSL), Créteil, France

[8]Centre National de Recherches Météorologiques, Météo-France, Toulouse, URA1357, France

[9]IERSD, National Observatory of Athens, P. Penteli, 15236, Athens, Greece

Correspondence to: Karine Sellegri (K.Sellegri@opgc.cnrs.fr)

Abstract. Over the last two decades, new particle formation (NPF), i.e. the formation of new particle clusters from gas-phase compounds followed by their growth to the 10-50 nm size range, has been extensively observed in the atmosphere at a given location, but their spatial extent rarely assessed. In this work, we use aerosol size distribution measurements performed simultaneously at Ersa (Corsica) and Finokalia (Crete) over a one-year period to analyze the occurrence of NPF events in the Mediterranean area. The geographical location of these two sites, as well as the extended sampling period allow us to assess the spatial and temporal variability of atmospheric nucleation at a regional scale. Finokalia and Ersa show similar seasonalities in the monthly average nucleation frequencies, growth rates, and nucleation rates although the two stations are located more than 1000 km away from each other. Within this extended period, aerosol size distribution measurements were performed during an intensive campaign (July 3rd to August 12th 2013) from a ground based station on the island of Mallorca, as well as onboard the ATR-42 research aircraft. This unique combination of stationary and mobile measurements provides us with detailed insights into the horizontal and vertical development of the NPF process on a daily scale. During the intensive campaign, nucleation events occurred simultaneously both at Ersa and Mallorca over delimited time slots of several days, but different features were observed at Finokalia. The results highlight that the spatial extent of the NPF events over the Mediterranean Sea might be as large as several hundreds of kilometers, mainly determined by synoptic conditions. Airborne measurements gave additional information regarding the origin of the clusters detected above the sea. The selected cases depicted contrasting

situations, with clusters formed in the marine boundary layer or initially nucleated above the continent or in the free troposphere (FT) and further transported above the sea.

1 Introduction

New particle formation (NPF) events have been widely observed in the atmosphere in different environments (Kulmala et al., 2004) from remote areas at high altitude or latitude to polluted environments in different climates (Pey et al., 2008; Manninen et al., 2010; Yli-Juuti et al., 2011; Cusack et al., 2013). However, the exact mechanism and chemical species involved in the NPF process are not fully identified, especially regarding the diversity of environments to consider. Thus, most global climate models still do not represent well this process, and use parameterizations which are based upon a limited number of mechanisms and gaseous precursors, even though they predict that it may contribute to a significant fraction of condensation nuclei (CN) and cloud condensation nuclei (CCN) concentration at the global scale (Spracklen et al., 2008; Merikanto et al., 2009; Makkonen et al., 2012).

The different features of NPF events (frequency, intensity, duration) may be influenced by meteorological variables (temperature, relative humidity and solar radiation) (Birmili et al., 2003; Jeong et al., 2004; Sihto et al., 2006; Young et al., 2007), but also by the availability of gaseous precursors, regarding both their nature and their amount. It is thus necessary to describe the occurrence and characteristics of NPF over a large variety of environments, and assess to what spatial extent these features can be applied to. Although the characteristics of the NPF events have often been documented in the literature (Hirsikko et al., 2007; Manninen et al., 2010; Yli-Juuti et al., 2009, 2011), analysis dedicated to their spatial extent are rarer. This might be explained by the fact that such studies require airborne measurements (Crumeyrolle et al. 2010; Rose et al., 2015a) or multi-sites datasets. Such datasets were analyzed by Vana et al. (2004) and Hussein et al. (2009) who reported that NPF could take place in the form of regional events over up to thousand kilometers in Scandinavia, and at least 500 kilometers over the western coast of Korea (Kim et al. 2016). Likewise, Dall'Osto et al. (2013) observed regional NPF events occurring in the north-east of Spain. Using a similar methodology, Crippa and Pryor, (2013) observed horizontal extents of a hundred kilometers for the NPF process in USA and Canada. They also pointed out a significant variability of the NPF characteristics (formation and growth rates) within these large-scale events, suggesting that local signatures could superimpose to favorable synoptic conditions. In order to allow for the analysis of the horizontal extent of NPF on a single station dataset, different methods based on air mass back trajectory analysis and particle growth rates were also recently proposed (Kristensson et al., 2014; Rose et al., 2015b). The Nanomap tool developed by Kristensson et al., (2014) was reported to allow the identification of nucleation areas up to 500 km away from the observation site. The main limitation of this last method is due to the fact that the determination of the nucleation area directly depends on event characteristics that sometimes cannot be accurately defined (i.e. the determination of the end of the nucleation process itself, or the end of the growth process).

These studies dedicated to the analysis of the horizontal extent of NPF were mainly conducted above continental regions. Similar analysis in marine environments are crucially missing although they are of high interest, as it was previously shown that in such pristine environments, cloud properties could be significantly impacted by changes in the aerosol loading (Tao et al., 2012; Koren et al., 2014; Rosenfeld et al., 2014). Although the

Mediterranean area is particularly sensitive to the future evolution of atmospheric pollutants and climate change, only a few studies related to NPF in this area have been reported so far. Intensive campaigns were conducted on the eastern Spanish coast, in Barcelona and at Montseny site (Pey et al., 2008; Cusack et al., 2013), while long-term measurements are performed at the Finokalia (Crete) station (Kalivitis et al., 2008, 2012, 2015; Manninen et al., 2010; Pikridas et al., 2012), where NPF event days are close to 30%. The Mediterranean basin is at the cross section of many different influences: there is a strong anthropogenic influence from densely populated coastal zones, which superimpose with marine and dust sources, as well as with emissions from Mediterranean forests and shrublands that emit both terpenes and isoprene. This geographical area is particularly exposed to high solar radiation compared to the rest of Europe, so that we expect a strong contribution from photochemical processes.

In the framework of the projects CHARMEX-ADRIMED (Mallet et al., 2015) and CHARMEX-SafMed, a large coordinated effort has been recently conducted to better characterize the physico-chemical properties of the Mediterranean atmosphere. Measurements were conducted at ground-stations on Mediterranean islands, such as Crete (Finokalia) and Corsica (Ersa) for an extended period of the years 2013-2014 and Mallorca (Cap Es Pinar) for several weeks during 2013. Forty research flights were also performed during the summers 2013 and 2014. This vast dataset gave us a unique opportunity to characterize the spatial extent of the NPF process in the Mediterranean basin. In this paper, we first report the long-term analysis of NPF event characteristics observed at Ersa (from May 2012 to August 2013) and Finokalia (from January to December 2013) using size distribution measurements in order to assess the large-scale space and time variability of NPF. We then focus our study on the Special Operation Period (SOP) that took place during summer 2013. During this SOP additional measurements were performed in Mallorca (from July 3rd to August 12th 2013) and aerosol particle size distributions and concentrations were measured onboard the ATR-42, which allowed for a deeper analysis of the horizontal and vertical development of the NPF process at daily scale.

2 Experimental platforms, material and methods

2.1 Ground-based measurements

Ground-based aerosol measurements reported in this work were performed at the Finokalia station (Crete) from January to December 2013, at the Ersa station (Corsica) from May 2012 to August 2013, and at the Cap Es Pinar station (Mallorca) from July 3rd to August 12th 2013 (Fig. 1). Within these measurements periods, some gaps occurred in the Finokalia dataset (from September 5th to October 15th 2013) due to participation of the instrument in the ACTRIS (Aerosol Clouds and Trace gases Research Infrastructure) network mobility particle size spectrometer workshop, and in the Ersa dataset (from September 1st to October 31th 2012) because of instrumental failures.

The Finokalia station (35.24° N, 25.60° E) is located on the northern coast of Crete, Greece, at the top of a hill (230 m a.s.l) facing the sea. There is no significant human activity within an area of approximately 15 km around the station, mainly characterized by a scarce vegetation (Mihalopoulos et al., 1997). The closest large urban area is the city of Heraklion, with 150 000 inhabitants, located 50 km west from Finokalia. Aerosols at the site are mainly transported from the south-eastern Europe and northern Africa, and to a lesser extent from central and

114 western Europe (Kouvarakis et al., 2000; Sciare et al., 2008; Pikridas et al., 2010, 2012). At Finokalia, aerosol
115 particle size distributions were measured in the size range 9 - 849 nm with a time resolution of 300 s with a
116 custom-made scanning mobility particle sizer (SMPS) (Wiedensohler et al., 2012). As previously described by
117 Kalivitis et al., (2015), the system operates with a closed-loop sheath air flow with a 5:1 ratio between the sheath
118 and the aerosol flow. It comprises a Kr-85 aerosol neutralizer (TSI 3077), a Hauke medium differential mobility
119 analyzer (DMA) and a TSI-3772 condensation particle counter (CPC). The system is operated following the
120 recommendations of Wiedensohler et al., (2012), thus meeting the European infrastructure ACTRIS project
121 requirements for quality insurance.

122 The Ersa station is located on the northern tip of Corsica Island, on Cape Corsica (43.00° N, 9.30° E, 530 m
123 a.s.l.). On this part of the island the wind can be very strong with frequent windstorms (78 days in 2007 with
124 wind speeds stronger than 28 m s^{-1}). Climate in Corsica is characterized by moist winters and dry summers, with
125 less than 100 rainy days per year (Lambert et al., 2009). Aerosols reaching the site are of variable types,
126 including mineral dust particles from north Africa, anthropogenic and biomass burning aerosols mainly
127 originating from densely populated coastal areas located in eastern Spain, France and Italy, and marine aerosols,
128 from the Mediterranean Sea itself but also from the Atlantic Ocean (Nabat et al., 2013; Mallet et al., 2016). The
129 Cape Corsica peninsula is a remote site, excluding important local anthropogenic sources that could affect the in-
130 situ measurements, and surrounded by a scarce Mediterranean vegetation (Mallet et al., 2016). At Ersa, aerosol
131 size distributions were measured with a scanning mobility particle sizer (SMPS TSI 3080, associated to a CPC
132 TSI 3010) in the size range 10 - 495 nm with a time resolution of 300 s.

133 The Cap Es Pinar station is located on the northeastern side of the Mallorca Island (39.88° N, 3.19° E, 20 m
134 a.s.l.), on a peninsula between the Alcudia and Pollença bays. The station was established in one of the buildings
135 belonging to the Spanish Ministry of Defense in its Cap Es Pinar facilities. The area is densely forested by
136 Mediterranean shrublands and pine trees and the access to the station is restricted. Urban centers, the Alcudia
137 and Pollença harbors and main roads are located at least 10 km from the site. Particle size distributions were
138 measured in the size range 15-600 nm with a time resolution of 300 s using a TSI SMPS, with a 3081 long DMA
139 and a CPC TSI 3776.

140 **2.2 Airborne measurements**

141 Airborne measurements were carried out onboard the ATR-42 French research aircraft operated by SAFIRE
142 (Service des Avions Français Instrumentés pour la Recherche en Environnement). Figure 1 shows the aircraft
143 trajectory during the flights performed on July 30th and August 1st which are investigated in the next sections of
144 the present work. The aerosol size distribution in the 20-485 nm diameter range was measured with a time
145 resolution of 130 s using the SMPS system previously described in Crumeyrolle et al. (2010) which includes a
146 CPC TSI 3010, a differential mobility analyser (DMA) and a krypton aerosol neutralizer. The total
147 concentrations of aerosols larger than 10 nm (N_{10}) and larger than 3 nm (N_3) were measured using a custom-
148 made CPC dedicated to aircraft measurements (Weigel et al., 2009) and a CPC TSI 3025, respectively. The
149 concentration of particles in the size range 3 - 10nm (N_{3-10}) was calculated as the difference between N_3 and N_{10}.
150 After analysis of the variability of N_{3-10} apart from nucleation periods, we found that N_{3-10} concentrations are
151 above the variability of the two CPC concentration difference when exceeding the threshold of 395 cm^{-3}. For

152 more details on the airborne instrumentation and data analysis procedure, the reader is referred to Rose et al.,
153 (2015a).

154

155 **3 Data analysis**

156 **3.1 NPF events classification**

157 From ground-based observations, measurement days were classified according to Dal Maso et al. (2005) into
158 four categories: events days, including classes I and II, undefined and non-events days. Class I events are
159 characterized by a strong increase of sub-25nm particles concentrations, their persistence over a period of more
160 than an hour and a clear growth of the nucleation mode particles towards larger sizes during the following hours.
161 Class II events have the same characteristics as Class I events, except that they may be less intense or show a
162 discontinuity in the growth of the clusters. Days are considered undefined when the newly observed particles are
163 detected only from the Aitken size and/or when they do not grow during the course of the day.

164 **3.2 Particle formation and growth rates calculations**

165 Particle formation and growth rates are key entities to assess the strength of events belonging to Class I and II.
166 While formation rates (J) are usually calculated for 10 nm particles (J_{10}), sampling line issues causing high
167 variability of the sub-16 nm concentrations in Cap Es Pinar (see Fig. 7) only allowed for calculations involving
168 larger diameter particle concentrations (J_{16}). In order to ease the comparison between Ersa and Cap Es Pinar, a
169 similar size range was applied for J calculation from the Ersa dataset. For comparison with the literature, one has
170 to keep in mind that J_{16} are lower than J_{10}, due to coagulation effects during the growth of the particles from 10
171 nm to 16 nm.

172 Growth rates (GR) were calculated from the SMPS nucleation mode concentrations (16-20 nm) using the
173 "maximum" method from Hirsikko et al.(2005). The time corresponding to the maximum concentration was first
174 determined for each of the SMPS size channels in the range 16 – 20 nm by fitting a normal distribution to the
175 concentration. The growth rate was then derived from a linear least square fit through these time values.

176 From this growth rate, we derived the total particle formation rate at 16 nm (J_{16}), similarly as in Dal Maso et
177 al. (2005) using the following equation (Eq.1) :

178 $$J16 = dN16dt + CoagS16 \times N16 + GR16 - 2020 - 16nm \times N16$$

179 (1)

180 $CoagS_{16}$ is the coagulation sink of 16 nm particles on larger particles, N_{16} is the total concentration of 16-20 nm
181 particles and GR_{16-20} is the growth rate corresponding to the same diameter range.

182

183 **4 Results and discussion**

184 **4.1 Yearly statistical analysis of NPF events characteristics at two ground-based stations**

185   The goal of this first section is to provide an overview of the seasonal variability of NPF in the Mediterranean
186   area, and some insights into the spatial homogeneity of the NPF occurrence over the basin.

4.1.1 NPF Events frequency and types

188   The yearly average NPF frequencies, calculated as the number of event days over the total number of
189   measurement days, are very similar at Finokalia and Ersa, being 36% (109 events) and 35% (96 events),
190   respectively (Table 1). A comparable value is reported by Pikridas et al. (2012) at Finokalia, with a yearly
191   average frequency of ~ 33% calculated over a year from April 2008 to April 2009. At both stations, the NPF
192   frequency shows a clear annual cycle with the highest frequencies observed during spring (52% in May for
193   Finokalia and 56% in April for Ersa), and the lowest in autumn (Fig. 2). A similar seasonal variation was
194   previously reported for Finokalia, with a slight time offset of the NPF frequency peak observed in February-
195   March (Pikridas et al., 2012). More generally, higher NPF frequencies are frequently observed during spring
196   (April-May-June) compared to the rest of the year at European stations (Manninen et al., 2010). As previously
197   suggested by Manninen et al. (2010, and references therein) and further supported by Fig. S1, higher NPF
198   frequencies in spring are most probably related to the onset of biogenic emissions which is favored by increasing
199   temperatures, together with higher solar radiation enhancing the production of low volatile oxidized vapors. The
200   classification of the event days into the different categories (Fig. 3 and Table 1) shows that the occurrence of
201   type I events in Finokalia follows the same seasonal variation as the total NPF frequency, being maximum
202   during the spring season (up to 26% of all days). This indicates that spring is favorable to both formation of new
203   particles and their growth to larger sizes. Type II events are annually the most frequent, representing between
204   13% and 31% of all measurement days with no clear seasonal variation. In contrast, undefined days are not
205   frequently observed in Finokalia, around 9% on average. Very similar features are observed in Ersa: type I
206   events show the highest frequency of occurrence during spring and summer (up to 32% of all days in August),
207   while they represent less than 10% of the measurement days during winter. The frequency of occurrence of type
208   II events is on average 19%, with no clear seasonal variation.

4.1.2 Growth rates and particle formation rates

210   Particle formation and growth rates were calculated for type I events in order to characterize the strength of
211   the events observed at the two stations. The yearly median particle growth rates in the range 16 – 20 nm (GR_{16-20})
212   are 7.10 and 16.7 nm h^{-1} at Ersa and Finokalia, respectively (Table 2). The values obtained at Finokalia are in
213   the upper range of the values reported by Manninen et al. (2010) at European sites for 7 – 20 nm diameter
214   particles (1.8 – 20 nm h^{-1}, mean value 4.4 nm h^{-1}). Especially, the values calculated in this work are on average
215   higher compared to those obtained at other European coastal sites such as Cabauw (2.1 - 19 nm h^{-1}, mean value
216   6.7 nm h^{-1}) and Mace Head (2.7 – 10 nm h^{-1}, mean year value 5.4 nm h^{-1}) (Manninen et al., 2010). Higher growth
217   rates are expected in environments with high solar radiation and emissions, such as the Mediterranean basin.
218   However, the median value reported here is also higher than the one reported for Finokalia from the years 2008-
219   2009 in the size range 7 – 20 nm (5 nm h^{-1}) (Manninen et al., 2010). This result may be explained by the higher
220   size range used here for the GR calculation (16-20nm instead of 7-20 nm), which leads to higher values because
221   GR usually increases with particle size, but also higher uncertainty because of the narrow size range. Figure 4
222   displays the annual variation of the particle growth rates at Ersa and Finokalia. At Ersa, GR have the same
223   seasonal variation as the NPF frequency, with higher values in spring compared to the rest of the year. At

224   Finokalia, the GR seasonality is not as clear as in Ersa. However, the seasonality in Finokalia is rather biased

225   because there are only few class I events during summer.

226   The yearly median particle formation rates (J_{16}) are 0.16 $cm^{-3}s^{-1}$ in Ersa and 0.26 $cm^{-3}s^{-1}$ in Finokalia (Table 2).

227   These values are slightly lower than the J_{10} values reported by Kulmala et al. (2004) from several coastal sites

228   and ship campaigns conducted in the Baltic, Atlantic and Pacific areas (0.4 – 1.5 $cm^{-3}s^{-1}$). Besides different

229   environmental conditions which might explain these differences, one has to keep in might that J_{16} values are

230   expected to be lower than J_{10} because of the coagulation processes which cause particle loss during their growth.

231   The values calculated in this work are, to our knowledge, the first reported for the formation of nucleation mode

232   particles (10 – 20 nm) in the Mediterranean basin. As shown on Fig. 5, median J_{16} also follows a seasonal

233   variation similar to the NPF frequency at both stations, with higher values in spring (March, with 0.56 $cm^{-3}s^{-1}$ for

234   Finokalia, and April, with 0.66 $cm^{-3}s^{-1}$ for Ersa). This observation suggests that condensable vapors needed to

235   grow the clusters up to 16 nm are most likely of the same origin as those initiating the NPF process. In contrast,

236   lower J_{16} are observed in early winter and mid-summer at both stations.

237   It is worth noticing that in Ersa, even though NPF frequencies are lower in autumn compared to spring,

238   particle formation rates are comparable. This last observation suggests that, despite being less frequent, favorable

239   conditions for NPF can be found during autumn and lead to events with the same intensity as in spring, when

240   radiation and biogenic emissions are on average higher compared to the rest of the year (Manninen et al., 2010).

241   The seasonal variation of nucleation frequency, nucleation rates and growth rates is most likely related the

242   availability of condensable gases. The amount of such precursors results from the balance between a

243   combination of emissions and radiation, that favor their production, and their loss onto preexisting particles. In

244   order to assess the influence of the preexisting aerosol population on NPF, we calculated the condensational sink

245   (CS) according to Pirjola et al. (1999). The CS was first derived from SMPS measurements for the whole

246   measurement period at both stations and was finally averaged over the two-hour period prior to the onset of NPF

247   events. On non-event days, the CS was averaged over the two-hours time period prior to the time at which NPF

248   is triggered on event days, i.e. ~ 11:00 (UTC) in Finokalia and ~ 12:00 (UTC) in Ersa. The annual variation of

249   the median CS derived from these averaged values is reported for event and non-event days on Fig. 6.

250   The CS has a strong seasonal cycle with a clear maximum during summer at both stations. This observation may

251   explain the lower NPF frequencies, formation rates and growth rates that are on average observed during this

252   season, that otherwise shows high radiation (Fig. S1), and most probably high biogenic emissions. In addition,

253   the CS is on average higher during non-event days at both stations. This confirms that the CS is likely a limiting

254   factor for the occurrence of NPF at these stations. This was already pointed out by Kulmala et al. (2005), Hamed

255   et al. (2010) and Manninen et al. (2010) for several boundary layer stations in Europe, including both

256   industrialized locations and more pristine areas, such as boreal forest. One should however note that during

257   spring months (especially March and April), median CS is similar on event and non-event days. This observation

258   suggests that during this period, the strength of precursors emissions together with radiation might be driving the

259   occurrence NPF to a major extent. Also, the CS is on average higher in Finokalia, especially during spring and

260   summer with monthly CS twice as high compared to Ersa. It is worth noticing that large particles up to 848 nm

261   are accounted for in the CS calculation in Finokalia, while the upper size limit is 495 nm in Ersa. However,

262   particles above 500 nm only have a weak impact on the Cs values due to their low concentration, and thus do not

263 explain the differences which are seen between the sites. At Finokalia, north-northeastern winds dominate during
264 summer, bringing high concentrations of anthropogenic aerosol that have aged when passing over the sea before
265 reaching the station, thus leading to high CS values. The fact that NPF frequencies, nucleation rates and growth
266 rates are comparable at the two stations indicates that the sources of condensable gases are likely to be
267 significantly higher in Finokalia compared to Ersa in order to compensate for the large condensational sink
268 measured at the Greek station.

269 Based on the previous observations, Finokalia and Ersa show similar seasonality in the average nucleation
270 frequency, growth rates and nucleation rates although the two stations are more than 1000 km away from each
271 other. It is worth mentioning that during the period of interest, 109 event days were observed at Finokalia and 96
272 at Ersa, among which 31 (with 8 events of class I) occurred at both stations at the same time. These results could
273 indicate that the spatial extent of NPF events over the Mediterranean basin is at the synoptic scale, and in the
274 order of the distance between the two stations, i.e. more than 1000 km. Such a conclusion was already drawn
275 from observations of NPF events at three stations located in northern Europe (Vana et al. 2004). However, we
276 will downscale the comparison of occurrence and characteristics of events at the daily resolution (rather than
277 monthly), in order to further investigate this hypothesis.

278 **4.2 Intensive campaign during summer 2013**

279 **4.2.1 Ground-based measurements - overview**

280 In this section, we focus on the Special Observation Period (SOP) that took place from June 3rd to August 12th in
281 the frame of the CHARMEX project. During this period, number size distribution measurements were
282 additionally conducted at the Mallorca station (Cap Es Pinar).

283 Figure 7 shows the SMPS particle size distributions recorded at the three ground-based stations during the SOP.
284 From this global overview, we clearly observe similar trends in the evolution of the particle size distributions in
285 Ersa and Cap Es Pinar, with three distinct NPF periods during which NPF events occurred daily over several
286 days (First period from July 4th to July 9th, second period from July 28th to August 3rd and third period from
287 August 9th to August 12th) (see Table S1). This observation would confirm the spatial extent of NPF events at a
288 large scale. However, these periods of intense NPF activity are not observed in Finokalia, where both the
289 occurrence and strength of NPF events seem to be more homogeneous over the SOP. These contrasting
290 observations might be explained by an environmental contrast between the eastern and western part of the
291 Mediterranean basin.

292 As reported in Table S1, during this 41-days period, NPF was observed to occur at one station (at least) on 23
293 days. Among these 23 event days, 8 events were observed on the same day on two stations at least. This
294 frequency of simultaneous NPF events occurrence is very similar to the one observed at Korean coastal sites (5
295 out of 21 observation days, Kim et al. 2016). NPF was detected at all sites on August 9th, and three events were
296 reported on the same day for each of the station pairs Ersa – Finokalia and Ersa – Mallorca, and one event for the
297 pair Finokalia - Mallorca. In order to further investigate the link that might exist between the events observed at
298 the three stations, we first chose to focus our analysis on three days that belong to the three different NPF periods
299 identified: July 5th, July 29th and August 9th are presented as case studies. Type one events were observed in Ersa

300 and Cap Es Pinar on those specific days, thus allowing for particle formation and growth rates calculations, and

301 further direct comparison of event intensity at these two sites.

302 **4.2.2 Ground-based measurements: Case studies**

303 We calculated the total formation rate of 20 nm particles (J_{20}) using particle growth rates in the size range 15-25

304 nm (GR_{15-25}, Table 3) for the three cases: July 5th, July 29th and August 9th. We first shortly describe the NPF

305 events observed on the 5th and 29th of July (fully described in the supplementary) and then illustrate in more

306 details the events observed on the 9th of august that have the most similarities between sites.

307 On July 5th, although NPF occurred both at Ersa and Cap Es Pinar, the time evolution of particle concentrations

308 are very different from one site to the other. Particles of the smallest size range are detected in the morning at

309 Ersa, but ony later in the afternoon at Cap es Pinar, and at larger sizes and lower concentrations (Fig. S2). The

310 24-hour air mass back trajectory analysis (HYSPLIT transport and dispersion model, Draxler et al. 2003) shows

311 that air masses arriving at both stations are of northerly origin (Fig. S3). Hence it is unlikely that particles formed

312 during the NPF event detected at Ersa in the morning have been transported west and detected later in the

313 afternoon at Cap Es Pinar.

314 In order to further evaluate the spatial extent of nucleation, we estimated for each site the distance between the

315 station the place where nucleation was initially triggered upstream the station. The method we used is based on

316 the time evolution of the aerosol size distribution and was previously described by Rose et al. (2015b). We

317 assumed that 20 nm particles detected at the station were originally formed by NPF and that nucleated clusters

318 had a diameter of 1 nm. The time required for a cluster to grow between 1 and 20 nm was first calculated using

319 GR_{15-25}. Then, knowing the time corresponding to the maximum concentration of 20 nm particles at the station,

320 we were able to calculate the time at which nucleation occurred. Finally, using air mass back trajectories we

321 determined the location where nucleation had been triggered upstream the station. It is worth noticing that since

322 particle growth rates were reported to increase with particle size (Yli-Juuti et al, 2011), GR_{15-25} provide an

323 underestimation of the particle growth time between 1 and 20 nm, and therefore a lower limit of the distance

324 between the place where nucleation is initially triggered and the station.

325 On July 5th, previous calculations lead to distances of at least 9 km (Ersa) and 40 km (Cap Es Pinar) upstream the

326 stations, which thus cannot allow further conclusions on the simultaneity of a large NPF covering the spatial area

327 of both stations. The event of July 29th was detected from the lowest sizes of the SMPS at both stations with the

328 same intensity (similar N_{15-20} and J_{20}), and show similar features (Fig. S4), but was detected one hour earlier at

329 Cap Es Pinar than at Ersa. Air masses were from the northern sector at Cap Es Pinar, and then turned west

330 towards Ersa (Fig. S6).

331 In Finokalia, both for July 5th and July 29th, significant N_{15-20} concentration are also detected during the

332 nucleation hours, but in the form of a succession of peaks that do not show the usual feature of a clear NPF event

333 (with a continuous growth).

334   On August 9th, newly formed particles are detected in air masses originating from the near southern area in Ersa

335 and from northwestern sector in Cap Es Pinar (see Fig.9). The concentration of particles mesured in the first

336 SMPS size channels in Ersa (11-15 nm) does not present very marked variations, while N_{15-20} displays more

significant changes in the course of the day. These observations might suggest that unlike previous events, NPF could not be initiated at the station itself, but rather in a neighbouring area (Fig. 8). Similar features are observed at Cap Es Pinar, with significant variations of the particle concentration in the size range 15-20 nm, as on July 29th. The temporal evolutions of N_{15-20} and N_{20-25} have similar structures at both stations between 10:00 and 16:00 UTC, suggesting that NPF could occur simultaneously at both sites. Additional peaks of N_{15-20} and N_{20-25} are detected earlier in the morning at Cap Es Pinar (7:20 and 9:00 UTC), while they are not detected in Ersa. Beside the simultaneity of the process, NPF events detected at the two sites also display very similar characteristics, both regarding particle growth (4.3 and 3.8 nm h^{-1}, for Ersa and Cap Es Pinar, respectively) and formation rates (4.83 and 4.17 cm^{-3} s^{-1}, for Ersa and Cap Es Pinar, respectively). Instrumental failure did not allow similar analysis at Finokalia.

As shown on Fig. 9 for Cap Es Pinar, the place where nucleation initially occurred was at least 49 km upstream the station. Since all air mass back trajectories computed during the time period of interest are very local (at least during the 24 hours before their arrival at the site), we may hypothesis that NPF is occuring over the whole area close to Mallorca where air mass backtrajectories overlap. Concerning Ersa, the nucleation of 20 nm particles latter observed at the site is at least initiated 45 km upstream the station.

The three case studies showed that NPF events could be detected, with some time offset, on two remote stations separated by several hundred kilometers in the Mediterranean area. In particular for the case of August 9th, the fact that these events can be detected in air masses from different origins suggest that the NPF is, for both sites, initiated above the sea, either in the marine boundary layer or higher in the free troposphere. In any case, the NPF process is likely not subject to the availablility of precursors that would be specific to the air mass type reaching the sites. It could rather depend on synoptic meteorological conditions at the European scale, including low condensational sinks following precipitations periods. Indeed, the analysis of the meteorological conditons along backtrajectories shows that precipitation did occur prior to their arrival at both stations on July 29th (during the passage of low pressure systems), but not on the two other case studies. The minimum areas that we determined for nucleation onset at both sites do not overlap. However, the estimates we obtained are some lower limits of the actual values, and there are no elements which could justify that the NPF is interrupted between both sites. Airborne measurements will be used in the next section to further investigate this aspect. In addition, these flights will allow an analysis regarding the origin of the clusters and their precursors, from the marine boundary layer or from the upper levels of the atmosphere, as previously shown by Rose et al. (2015a).

4.2.3 Airborne measurements

Among the 11 flights performed during the SOP period, particles in the lowest size range (N_{3-10}) were not observed during 7 of the flights, in agreement with no NPF events detected at the Ersa and Cap Es Pinar stations. Two flights detected elevated concentrations of N_{3-10} and N_{10-20} in agreement with NPF events at Ersa.

The first event to be investigated was observed on July 30th. Regarding aircraft measurements, the analysis was focused on the flight legs performed at constant altitude and during which N_{3-10} concentrations were above the threshold value (Fig. 10a). The first part of the flight was performed at low altitude ($\sim$ 215 m a.s.l.) from the french coast towards Ersa and at higher altitudes ($\sim$ 3400 m a.s.l.) during the second part of the flight from Ersa towards the coast. Based on Fig. 10, small particles (N_{3-10}) were detected at both altitudes and over a large area

375 included in a 219 × 131 km rectangle. On the low altitude flight section, N_{3-10} are decreasing from the
376 northeastern part of the flight track to the southwestern one. This would indicate a source of nanoparticles
377 originating from the continent and progressively diluted in the marine boundary layer. However, despite a high
378 variability, N_{3-10} were on average higher at high altitude, with average concentrations of 3805 ± 1555 cm^{-3}
379 compared to 2040 ± 2174 cm^{-3} at lower altitude. This last observation supports the results of Rose et al. (2015a)
380 who reported that nucleation could be enhanced at high altitude above the Mediterranean Sea and connected to
381 different sources at low altitude.

382 In order to explore the link that may exist between the events detected simultaneously from the aircraft and from
383 the ground, we first investigated the origin of the air masses. Figure 10b shows the 72 hour back trajectories of
384 the air masses sampled by the ATR-42 every 10 min along the flight path as well as the 72 hour back trajectories
385 of the air masses that reached Ersa in the meanwhile at 13:00, 14:00 and 15:00 UTC. During the first part of the
386 flight performed at low altitude, the aircraft flew in southern air masses which all passed over the continent
387 before sampling and became more local as the aircraft approached Ersa. In contrast, the air masses sampled at
388 high altitude were from western origin, so that they also passed over the continent, but did not display any local
389 features.

390 In addition, Fig. 11 shows the evolution of the particle size distributions measured onboard the ATR-42 and at
391 Ersa. The spectra are color coded according to the position of the aircraft indicated in the insert included in the
392 middle panel of Fig. 11. At Ersa, the shape of the particle size distribution remains similar during the whole
393 measurement period, with a nucleation mode around 20 – 25 nm, an Aitken mode around 50 – 60 nm which
394 clearly dominates the spectra and two accumulation modes, respectively around 110 and 220 nm. These modes
395 were identified when fitting the SMPS size distributions with four Gaussian modes using the methodology
396 described in Rose et al. (2015a). In contrast, the size distributions provided by the SMPS onboard the ATR-42
397 show significant variations. Lower concentrations are on average observed at higher altitude for the whole
398 diameter range but with more significant changes of the nucleation and Aitken modes. The shape of the size
399 distribution is also impacted by the location of the plane, especially at low altitude. In fact, the total particle
400 concentration decreases as the aircraft moves further off the southern coast of France, with, again, a more visible
401 impact on nucleation and Aitken modes.

402 These last observations, together with the air mass back trajectory analysis shown on Fig. 10.b, suggest that for
403 this first event, new particles were initially formed at low altitude over the continent and further transported
404 above the sea to be finally detected over a large area, and more especially in Ersa. Decreasing particle
405 concentrations observed while moving further off the continent make less probable the hypothesis of new small
406 particles formation from an additional marine source, but rather depict the effect of dispersion process that may
407 have taken place during particle transport.

408 The second event included in this analysis was observed on August 1st. Compared to the previous case study, the
409 flight was performed over a larger area (172 × 247 km rectangle) located further away west from Ersa and at a
410 relatively low constant altitude (~ 500 m a.s.l.). N_{3-10} concentrations above the threshold value were detected
411 along the flight path (Fig. 12) and compared well, on average, with the concentrations obtained at low altitude
412 during the flight performed on July 30th (2483 ± 2767 cm^{-3}). However, N_{3-10} concentrations occurred as bursts,
413 with no clear spatial gradient as previously reported for flight performed on July 30th. The analysis of air mass

414 back trajectories is shown on Fig 12.b. north-eastern air masses were sampled at the beginning and at the end of
415 the flight, with northern air masses in between. Air masses from the north were also detected at Ersa and it is
416 worth noticing that, at least during the first part of the flight, the air masses that reached the aircraft had all
417 passed over Ersa region.

418 The evolution of the particle size distributions together with the location of the aircraft is shown in Fig. 13.
419 Unlike during the flight performed on July 30th, the shape of the distributions measured onboard the ATR-42
420 remains similar during the whole measurement period despite the changing origin of air masses. In contrast, the
421 shape of the particle size distributions measured at Ersa shows a significant variability. Especially, the nucleation
422 mode displays increasing diameters from 20 to 30 nm and highly variable concentrations. Also, total
423 concentrations from Ersa are significantly higher compared to those measured onboard the ATR-42.

424 In order to further investigate the origin of the nucleation mode particles and the connection that may exist
425 between ground based and airborne measurements, we compared the diameters of the corresponding nucleation
426 modes. For that purpose, Fig. 14 shows the ratio of the nucleation mode diameter obtained onboard the ATR-42
427 over that from Ersa as a function of the distance between the aircraft and the station. This ratio is in the range 0.6
428 – 1.2, with on average decreasing values while increasing the distance between the two measurement points.
429 Nucleation mode diameter getting smaller along the air mass back trajectory above the sea could be the result of
430 intense inputs of nucleated particles initially below the SMPS size detection limit and feeding the nucleation
431 mode as they grow, as confirmed by the occurrence of N_{3-10} nm particles detected in the ATR-42. In this
432 particular case, particles detected in the nucleation mode observed onboard the ATR-42 would be the result of an
433 event occurring above the sea from marine precursors, which superimposes with a preexisting particle mode.

434

435 **5 Conclusion**

436 We investigated the occurrence of NPF in the Mediterranean area using particle size distributions measured at
437 three ground-based stations (Ersa, Cap Es Pinar and Finokalia) as well as airborne measurements performed in
438 2013 in the frame of the CHARMEX-ADRIMED and CHARMEX-SafMed projects.

439 The analysis of long-term datasets from Ersa and Finokalia first revealed similar features, although the two
440 stations are more than 1000 km away from each other. Especially, almost equal annual NPF frequencies were
441 reported (36% and 35%, for Finokalia and Ersa, respectively) and similar seasonal variations of both the NPF
442 frequency and characteristics, i.e. particle formation and growth rates, were observed. The NPF process was on
443 average favored during spring, both in terms of occurrence and intensity, most probably because of increased
444 amounts of precursors from biogenic origin and higher solar radiation, thus allowing for more efficient
445 photochemistry processes.

446 This investigation, initially performed at a monthly resolution was downscaled in a second step at the daily
447 resolution over a two months period, in order to further assess the simultaneity of NPF over a large part of the
448 Mediterranean basin. Three simultaneous nucleation periods of several days appeared clearly for Ersa and Cap
449 Es Pinar, and less clearly at Finokalia. NPF formation was observed to occur simultaneously at least at two of the
450 three stations on 8 days over the 41 days of observation, which confirms the frequent occurrence of regional

451 scale NPF events in the Mediterranean area. Three case study events were selected within these three distinct
452 NPF periods for a more detailed analysis. These three case studies showed that NPF events could be detected,
453 with some time offset, on two remote stations separated by several hundred kilometers in the Mediterranean
454 basin, without the stations being directly linked to eachother within a single air mass trajectory. While featuring
455 local characteristics, the occurrence of NPF events was likely not dependant on the availablility of precursors
456 that would be specific to the air mass type reaching the sites, but rather on synoptic meteorological conditions at
457 the European scale. Kompula et al. (2006) also concluded from observation from two different sites 250 km
458 appart, that the occurrence of of NPF in a certain air mass type depended not only on the local conditions
459 promoting the process (such as photochemistry), but also on some properties carried by the air mass itself.
460 Likewise, Hussein et al. (2009) showed from a multisites observations dataset in Scandinavia that although large
461 spatial scale NPF events were observed simultaneously bewteen several stations, their characteristics usually
462 differ in term of temporal evolution, due to different local meteorological conditions, and maybe variable local
463 emissions.

464 The case studies also showed that despite the fact that nucleation monthly frequencies, monthly nucleation rates
465 and growth rates had similar seasonnal variations in Ersa and Finokalia, different behaviors were observed on a
466 daily basis between the western and eastern mediterranean bassins. Again, the combination of favourable
467 synoptic conditions and seasonnal variations in general emission schemes may favour a seasonnal behavior of
468 the NPF frequency and characteristics, but local conditions are modulating the general behavior of regional NPF.

469 Airborne measurements were finally used to further investigate the horizontal and vertical extent of NPF, and to
470 determine the origin of the clusters and their precursors. Two case studies were again selected within the NPF
471 periods identified previously from ground-based observations, during which newly formed clusters were
472 observed onboard the ATR-42 and from Ersa on the same day. Airborne measurements confirmed the regional
473 spatial extend of NPF events, and further showed regional NPF events can have different sources. The selected
474 events depicted contrasting situations where particles were initially probably formed above the continent for one
475 of them, both in the boundary layer and in the free troposphere, and probably formed above the sea for the other.

476 This work, together with the previous study by Rose et al. (2015a), demonstrates the occurrence of NPF in the
477 Mediterranean basin, thus highlighting the possibility for the process to be triggered above open seas. Those
478 results are of great interest to improve the parameterizations of nucleation in models, which actually only
479 consider a limited number of precursors, commonly including sulfuric acid and ammonia but excluding those
480 more specifically emitted in the marine atmosphere. Model predictions would also benefit from the analysis of
481 the vertical extent of the NPF process provided in these studies. Besides the identification of preferential
482 altitudes for the occurrence of the process, these results aid understanding the transport of the newly formed
483 clusters and their precursors between the boundary layer and the free troposphere. Future studies should focus on
484 understanding the chemical precursors that contribute to these new particle formation processes.

485 **Ackowledgements**

486 This study was performed with the financial support of the French National Research Agency (ANR) project
487 ADRIMED (contract ANR-11-BS56-0006) the ANR project SAf-Med "" (Grant Number: SIMI-5-6 022 04) and
488 is part of the ChArMEx project supported by ADEME, CEA, CNRS-INSU and Météo-France through the
489 multidisciplinary programme MISTRALS (Mediterranean Integrated Studies aT Regional And Local

Scales). The Financial support for the ACTRIS Research Infrastructure Project by the European Union's Horizon 2020 research and innovation program under grant agreement no. 654169 and previously Under grant agreement no. 262254 in the 7th Framework Programme (FP7/2007–2013) is gratefully acknowledged.

References

Birmili, W., Berresheim, H., Plass-Dülmer, C., Elste, T., Gilge, S., Wiedensohler, A. and Uhrner, U.: The Hohenpeissenberg aerosol formation experiment (HAFEX): a long-term study including size-resolved aerosol, H 2 SO 4, OH, and monoterpenes measurements, Atmospheric Chem. Phys., 3(2), 361–376, 2003.

Crippa, P. and Pryor, S. C.: Spatial and temporal scales of new particle formation events in eastern North America, Atmos. Environ., 75, 257–264, doi:10.1016/j.atmosenv.2013.04.051, 2013.

Crumeyrolle, S., Manninen, H. E., Sellegri, K., Roberts, G., Gomes, L., Kulmala, M., Weigel, R., Laj, P. and Schwarzenboeck, A.: New particle formation events measured on board the ATR-42 aircraft during the EUCAARI campaign, Atmospheric Chem. Phys., 10(14), 6721–6735, doi:10.5194/acp-10-6721-2010, 2010.

Cusack, M., Pérez, N., Pey, J., Alastuey, A. and Querol, X.: Source apportionment of fine PM and sub-micron particle number concentrations at a regional background site in the western Mediterranean: a 2.5 year study, Atmospheric Chem. Phys., 13(10), 5173–5187, doi:10.5194/acp-13-5173-2013, 2013.

Dal Maso, M., Kulmala, M., Riipinen, I., Wagner, R., Hussein, T., Aalto, P. P. and Lehtinen, K. E. J.: Formation and growth of fresh atmospheric aerosols : eight years of aerosol size distribution data from SMEAR II, Hyytiälä, Finland, Boreal Environ. Res., 10(5), 323–336, 2005.

Dall'Osto, M., Querol, X., Alastuey, A., O'Dowd, C., Harrison, R. M., Wenger, J. and Gómez-Moreno, F. J.: On the spatial distribution and evolution of ultrafine particles in Barcelona, Atmospheric Chem. Phys., 13(2), 741–759, doi:10.5194/acp-13-741-2013, 2013.

Draxler, R. R. and Rolph, G. D.: HYSPLIT (Hybrid Single-Particle Langrangian Integrated Trajectory) Model access via NOAA ARL READY website (http://www.arl.noaa.gov/ready/hysplit4.html), 2003.

Hamed, A., Birmili, W., Joutsensaari, J., Mikkonen, S., Asmi, A., Wehner, B., Spindler, G., Jaatinen, A., Wiedensohler, A., Korhonen, H. and others: Changes in the production rate of secondary aerosol particles in Central Europe in view of decreasing SO 2 emissions between 1996 and 2006, Atmospheric Chem. Phys., 10(3), 1071–1091, 2010.

Hirsikko, A., Laakso, L., Hörrak, U., Aalto, P. P., Kerminen, V.-M. and Kulmala, M.: Annual and size dependent variation of growth rates and ion concentrations in boreal forest, Boreal Environ. Res., 10(5), 357–369, 2005.

Hirsikko, A., Bergman, T., Laakso, L., Maso, M. D., Riipinen, I., Horrak, U. and Kulmala, M.: Identification and classification of the formation of intermediate ions measured in boreal forest, Atmospheric Chem. Phys., 7(1), 201–210, 2007.

Hussein, T., Junninen, H., Tunved, P., Kristensson, A., Dal Maso, M., Riipinen, I., Aalto, P. P., Hansson, H.-C., Swietlicki, E. and Kulmala, M.: Time span and spatial scale of regional new particle formation events over Finland and Southern Sweden, Atmos Chem Phys, 9(14), 4699–4716, 2009.

Jeong, C.-H., Hopke, P. K., Chalupa, D. and Utell, M.: Characteristics of Nucleation and Growth Events of Ultrafine Particles Measured in Rochester, NY, Environ. Sci. Technol., 38(7), 1933–1940, doi:10.1021/es034811p, 2004.

Kalivitis, N., Birmili, W., Stock, M., Wehner, B., Massling, A., Wiedensohler, A., Gerasopoulos, E. and Mihalopoulos, N.: Particle size distributions in the Eastern Mediterranean troposphere, Atmospheric Chem. Phys., 8(22), 6729–6738, 2008.

Kalivitis, N., Stavroulas, I., Bougiatioti, A., Kouvarakis, G., Gagné, S., Manninen, H. E., Kulmala, M. and Mihalopoulos, N.: Night-time enhanced atmospheric ion concentrations in the marine boundary layer, Atmospheric Chem. Phys., 12(8), 3627–3638, doi:10.5194/acp-12-3627-2012, 2012.

537 Kalivitis, N., Kerminen, V.-M., Kouvarakis, G., Stavroulas, I., Bougiatioti, A., Nenes, A., Manninen, H. E.,
538 Petäjä, T., Kulmala, M. and Mihalopoulos, N.: Atmospheric new particle formation as a source of CCN in the
539 eastern Mediterranean marine boundary layer, Atmos Chem Phys, 15(16), 9203–9215, doi:10.5194/acp-15-9203-
540 2015, 2015.

541 Kim, Y., Kim, S.-W., Yoon, S.-C., Park, J.-S., Lim, J.-H., Hong, J., Lim, H.-C., Ryu, J., Lee, C.-K. and Heo,
542 B.-H.: Characteristics of formation and growth of atmospheric nanoparticles observed at four regional
543 background sites in Korea, Atmos. Res., 168, 80-91, doi.org/10.1016/j.atmosres.2015.08.020, 2016.

544 Komppula, M., Sihto, S.-L., Korhonen, H., Lihavainen, H., Kerminen, V.-M., Kulmala, M., and Viisanen, Y.:
545 New particle formation in air mass transported between two measurement sites in Northern Finland, Atmos.
546 Chem. Phys., 6, 2811-2824, doi:10.5194/acp-6-2811-2006, 2006.

547 Koren, I., Dagan, G., Altaratz, O. and others: From aerosol-limited to invigoration of warm convective clouds,
548 Science, 344(6188), 1143–1146, 2014.

549 Kouvarakis, G., Tsigaridis, K., Kanakidou, M. and Mihalopoulos, N.: Temporal variations of surface regional
550 background ozone over Crete Island in the southeast Mediterranean, J. Geophys. Res. Atmospheres 1984–2012,
551 105(D4), 4399–4407, 2000.

552 Kristensson, A., Johansson, M., Swietlicki, E., Kivekäs, N., Hussein, T., Nieminen, T., Kulmala, M. and Dal
553 Maso, M.: NanoMap: Geographical mapping of atmospheric new particle formation through analysis of 1
554 particle number size distribution data 2 3 Short version of title:"NanoMap: Mapping of new particle formation
555 events" 4 5, [online] Available from: http://www.cast.lu.se/Kristensson%20-%20NanoMap%20paper%20v4.pdf
556 (Accessed 14 March 2016), 2014.

557 Kulmala, M., Vehkamäki, H., Petäjä, T., Dal Maso, M., Lauri, A., Kerminen, V.-M., Birmili, W. and McMurry,
558 P. H.: Formation and growth rates of ultrafine atmospheric particles: a review of observations, J. Aerosol Sci.,
559 35(2), 143–176, 2004.

560 Kulmala, M., Petäjä, T., Mönkkönen, P., Koponen, I. K., Dal Maso, M., Aalto, P. P., Lehtinen, K. E. J. and
561 Kerminen, V.-M.: On the growth of nucleation mode particles: source rates of condensable vapor in polluted and
562 clean environments, Atmos Chem Phys, 5, 409–416, 2005.

563 Makkonen, R., Asmi, A., Kerminen, V.-M., Boy, M., Arneth, A., Hari, P. and Kulmala, M.: Air pollution control
564 and decreasing new particle formation lead to strong climate warming, Atmospheric Chem. Phys., 12(3), 1515–
565 1524, doi:10.5194/acp-12-1515-2012, 2012.

566 Mallet, M., Dulac, F., Formenti, P., Nabat, P., Sciare, J., Roberts, G., Pelon, J., Ancellet, G., Tanré, D., Parol, F.,
567 Denjean, C., Brogniez, G., di Sarra, A., Alados-Arboledas, L., Arndt, J., Auriol, F., Blarel, L., Bourrianne, T.,
568 Chazette, P., Chevaillier, S., Claeys, M., D'Anna, B., Derimian, Y., Desboeufs, K., Di Iorio, T., Doussin,
569 J.-F., Durand, P., Féron, A., Freney, E., Gaimoz, C., Goloub, P., Gómez-Amo, J. L., Granados-Muñoz, M. J.,
570 Grand, N., Hamonou, E., Jankowiak, I., Jeannot, M., Léon, J.-F., Maillé, M., Mailler, S., Meloni, D., Menut, L.,
571 Momboisse, G., Nicolas, J., Podvin, T., Pont, V., Rea, G., Renard, J.-B., Roblou, L., Schepanski, K.,
572 Schwarzenboeck, A., Sellegri, K., Sicard, M., Solmon, F., Somot, S., Torres, B., Totems, J., Triquet, S., Verdier,
573 N., Verwaerde, C., Waquet, F., Wenger, J. and Zapf, P.: Overview of the Chemistry-Aerosol Mediterranean
574 Experiment/Aerosol Direct Radiative Forcing on the Mediterranean Climate (ChArMEx/ADRIMED) summer
575 2013 campaign, Atmospheric Chem. Phys., 16(2), 455–504, doi:10.5194/acp-16-455-2016, 2016.

576 Manninen, H. E., Nieminen, T., Asmi, E., Gagné, S., Häkkinen, S., Lehtipalo, K., Aalto, P., Vana, M., Mirme,
577 A., Mirme, S., Hõrrak, U., Plass-Dülmer, C., Stange, G., Kiss, G., Hoffer, A., Törő, N., Moerman, M., Henzing,
578 B., de Leeuw, G., Brinkenberg, M., Kouvarakis, G. N., Bougiatioti, A., Mihalopoulos, N., O'Dowd, C.,
579 Ceburnis, D., Arneth, A., Svenningsson, B., Swietlicki, E., Tarozzi, L., Decesari, S., Facchini, M. C., Birmili,
580 W., Sonntag, A., Wiedensohler, A., Boulon, J., Sellegri, K., Laj, P., Gysel, M., Bukowiecki, N., Weingartner, E.,
581 Wehrle, G., Laaksonen, A., Hamed, A., Joutsensaari, J., Petäjä, T., Kerminen, V.-M. and Kulmala, M.:
582 EUCAARI ion spectrometer measurements at 12 European sites – analysis of new particle formation events,
583 Atmos Chem Phys, 10(16), 7907–7927, doi:10.5194/acp-10-7907-2010, 2010.

584 Merikanto, J., Spracklen, D. V., Mann, G. W., Pickering, S. J. and Carslaw, K. S.: Impact of nucleation on global
585 CCN, Atmospheric Chem. Phys., 9(21), 8601–8616, 2009.

586 Mihalopoulos, N., Stephanou, E., Kanakidou, M., Pilitsidis, S. and Bousquet, P.: Tropospheric aerosol ionic
587 composition in the Eastern Mediterranean region, Tellus, 49B, 314–326, 1997.

588 Nabat, P., Somot, S., Mallet, M., Chiapello, I., Morcrette, J. J., Solmon, F., Szopa, S., Dulac, F., Collins, W.,
589 Ghan, S., Horowitz, L. W., Lamarque, J. F., Lee, Y. H., Naik, V., Nagashima, T., Shindell, D. and Skeie, R.: A
590 4-D climatology (1979–2009) of the monthly tropospheric aerosol optical depth distribution over the
591 Mediterranean region from a comparative evaluation and blending of remote sensing and model products,
592 Atmospheric Meas. Tech., 6(5), 1287–1314, doi:10.5194/amt-6-1287-2013, 2013.

593 Pey, J., Rodríguez, S., Querol, X., Alastuey, A., Moreno, T., Putaud, J. P. and Van Dingenen, R.: Variations of
594 urban aerosols in the western Mediterranean, Atmos. Environ., 42(40), 9052–9062,
595 doi:10.1016/j.atmosenv.2008.09.049, 2008.

596 Pikridas, M., Bougiatioti, A., Hildebrandt, L., Engelhart, G. J., Kostenidou, E., Mohr, C., Prévôt, A. S. H.,
597 Kouvarakis, G., Zarmpas, P., Burkhart, J. F., Lee, B.-H., Psichoudaki, M., Mihalopoulos, N., Pilinis, C., Stohl,
598 A., Baltensperger, U., Kulmala, M. and Pandis, S. N.: The Finokalia Aerosol Measurement Experiment – 2008
599 (FAME-08): an overview, Atmospheric Chem. Phys., 10(14), 6793–6806, doi:10.5194/acp-10-6793-2010, 2010.

600 Pikridas, M., Riipinen, I., Hildebrandt, L., Kostenidou, E., Manninen, H., Mihalopoulos, N., Kalivitis, N.,
601 Burkhart, J. F., Stohl, A., Kulmala, M. and Pandis, S. N.: New particle formation at a remote site in the eastern
602 Mediterranean, J. Geophys. Res. Atmospheres, 117(D12), D12205, doi:10.1029/2012JD017570, 2012.

603 Pirjola, L., Kulmala, M., Wilck, M., Bischoff, A., Stratmann, F. and Otto, E.: Formation of sulphuric acid
604 aerosols and cloud condensation nuclei: an expression for significant nucleation and model comparison, J.
605 Aerosol Sci., 30(8), 1079–1094, doi:10.1016/S0021-8502(98)00776-9, 1999.

606 Rose, C., Sellegri, K., Freney, E., Dupuy, R., Colomb, A., Pichon, J.-M., Ribeiro, M., Bourianne, T., Burnet, F.
607 and Schwarzenboeck, A.: Airborne measurements of new particle formation in the free troposphere above the
608 Mediterranean Sea during the HYMEX campaign, Atmospheric Chem. Phys., 15(17), 10203–10218,
609 doi:10.5194/acp-15-10203-2015, 2015a.

610 Rose, C., Sellegri, K,, Velarde, F., Moreno, I., Ramonet, M., Weinhold,, K., Krejci, R., Andrade, M.,
611 Wiedensohler, A., and Laj, P.: Multiple daytime nucleation events at the high altitude station of Chacaltaya
612 (5240 m a.s.l.), Bolivia, Atmos. Environ., 102, 18–29, doi:10.1016/j.atmosenv.2014.11.015, 2015b.

613 Rosenfeld, D., Sherwood, S., Wood, R. and Donner, L.: Climate Effects of Aerosol-Cloud Interactions, Science,
614 343(6169), 379–380, doi:10.1126/science.1247490, 2014.

615 Sihto, S.-L., Kulmala, M., Kerminen, V.-M., Maso, M. D., Petäjä, T., Riipinen, I., Korhonen, H., Arnold, F.,
616 Janson, R., Boy, M. and others: Atmospheric sulphuric acid and aerosol formation: implications from
617 atmospheric measurements for nucleation and early growth mechanisms, Atmospheric Chem. Phys., 6(12),
618 4079–4091, 2006.

619 Sciare, J., K. Oikonomou, O. Favez, Z. Markaki, E. Liakakou, H. Cachier, and N.Mihalopoulos, Long-term
620 measurements of carbonaceous aerosols in the Eastern Mediterranean: Evidence of long-range transport of
621 biomass burning, Atmos. Chem. Phys., 8, 5551-5563, 2008

622 Spracklen, D. V., Carslaw, K. S., Kulmala, M., Kerminen, V.-M., Sihto, S.-L., Riipinen, I., Merikanto, J., Mann,
623 G. W., Chipperfield, M. P., Wiedensohler, A., Birmili, W. and Lihavainen, H.: Contribution of particle formation
624 to global cloud condensation nuclei concentrations, Geophys. Res. Lett., 35(6), doi:10.1029/2007GL033038,
625 2008.

626 Tao, W.-K., Chen, J.-P., Li, Z., Wang, C. and Zhang, C.: Impact of aerosols on convective clouds and
627 precipitation, Rev. Geophys., 50(2), doi:10.1029/2011RG000369, 2012.

628 Vana, M., Kulmala, M., Dal Maso, M., Hõrrak, U., and Tammet E.: Comparative study of nucleation mode
629 aerosol particles and intermediate air ions formation events at three sites, J. Geophys. Res., 109, D17201,
630 doi:10.1029/2003JD004413, 2004.

631   Weigel, R., Hermann, M., Curtius, J., Voigt, C., Walter, S., Böttger, T., Lepukhov, B., Belyaev, G. and
632   Borrmann, S.: Experimental characterization of the COndensation PArticle counting System for high altitude
633   aircraft-borne application, Atmospheric Meas. Tech., 2, 243–258, 2009.

634   Wiedensohler, A., Birmili, W., Nowak, A., Sonntag, A., Weinhold, K., Merkel, M., Wehner, B., Tuch, T.,
635   Pfeifer, S., Fiebig, M., Fjäraa, A. M., Asmi, E., Sellegri, K., Depuy, R., Venzac, H., Villani, P., Laj, P., Aalto, P.,
636   Ogren, J. A., Swietlicki, E., Williams, P., Roldin, P., Quincey, P., Hüglin, C., Fierz-Schmidhauser, R., Gysel, M.,
637   Weingartner, E., Riccobono, F., Santos, S., Grüning, C., Faloon, K., Beddows, D., Harrison, R., Monahan, C.,
638   Jennings, S. G., O'Dowd, C. D., Marinoni, A., Horn, H.-G., Keck, L., Jiang, J., Scheckman, J., McMurry, P. H.,
639   Deng, Z., Zhao, C. S., Moerman, M., Henzing, B., de Leeuw, G., Löschau, G. and Bastian, S.: Mobility particle
640   size spectrometers: harmonization of technical standards and data structure to facilitate high quality long-term
641   observations of atmospheric particle number size distributions, Atmospheric Meas. Tech., 5(3), 657–685,
642   doi:10.5194/amt-5-657-2012, 2012.

643   Yli-Juuti, T., Riipinen, I., Aalto, P. P., Nieminen, T., Maenhaut, W., Janssens, I. A., Claeys, M., Salma, I.,
644   Ocskay, R. and Hoffer, A.: Characteristics of new particle formation events and cluster ions at K-puszta,
645   Hungary, Boreal Environ. Res., 14(4), 683–698, 2009.

646   Yli-Juuti, T., Nieminen, T., Hirsikko, A., Aalto, P. P., Asmi, E., Hõrrak, U., Manninen, H. E., Patokoski, J., Dal
647   Maso, M., Petäjä, T., Rinne, J., Kulmala, M. and Riipinen, I.: Growth rates of nucleation mode particles in
648   Hyytiälä during 2003-2009: variation with particle size, season, data analysis method and ambient conditions,
649   Atmospheric Chem. Phys., 11(24), 12865–12886, doi:10.5194/acp-11-12865-2011, 2011.

650   Young, L.-H., Benson, D. R., Montanaro, W. M., Lee, S.-H., Pan, L. L., Rogers, D. C., Jensen, J., Stith, J. L.,
651   Davis, C. A., Campos, T. L., Bowman, K. P., Cooper, W. A. and Lait, L. R.: Enhanced new particle formation
652   observed in the northern midlatitude tropopause region, J. Geophys. Res., 112(D10),
653   doi:10.1029/2006JD008109, 2007.

654

654

655

Tables

657 Table 1 Classification of measurement days in Ersa and Finokalia (after filtering bad data).

	Number of measurements days	Event days		Undefined days	Non-event days
		Type I	Type II		
Ersa	276	43	53	23	157
Finokalia	301	38	71	27	165

658

659

660 Table 2 Annual median formation rates, growth rates and annual Cs in Ersa and Finokalia. Percentiles
661 are also reported as additional information.

	J_{16} (cm^{-3} s^{-1})			GR_{16-20} (nm h^{-1})			CS (s^{-1})		
	25th perc.	Med.	75th perc.	25th perc.	Med.	75th perc.	25th perc.	Med.	75th perc.
Ersa	1.4×10^{-1}	1.6×10^{-1}	3.0×10^{-1}	6.6	7.1	12.2	3.3×10^{-3}	4.1×10^{-3}	4.6×10^{-3}
Finokalia	1.9×10^{-1}	2.6×10^{-1}	2.8×10^{-1}	10.4	16.7	25.6	3.4×10^{-3}	6.2×10^{-3}	9.3×10^{-3}

662

663

664 Table 3 Average growth rates and formation rates computed for the three case studies at Ersa and Cap
665 Es Pinar.

	Ersa		Cap Es Pinar	
	GR_{15-25} (nm h^{-1})	J_{20} (cm^{-3} s^{-1})	GR_{15-25} (nm h^{-1})	J_{20} (cm^{-3} s^{-1})
July 5th	16.4	2.4×10^{-1}	7.8	4.1×10^{-2}
July 29th	8.9	7.9×10^{-2}	4.8	7.8×10^{-2}
August 9th	4.3	4.8×10^{-2}	3.8	4.2×10^{-2}

666

667

667

 Figures

669

671   Figure 1: Localization of the stations: Ersa (Corsica), Finokalia (Crete) and Cap Es Pinar (Mallorca).
672   Aircraft flight paths from July 30th and August 1st are also shown.

673

674
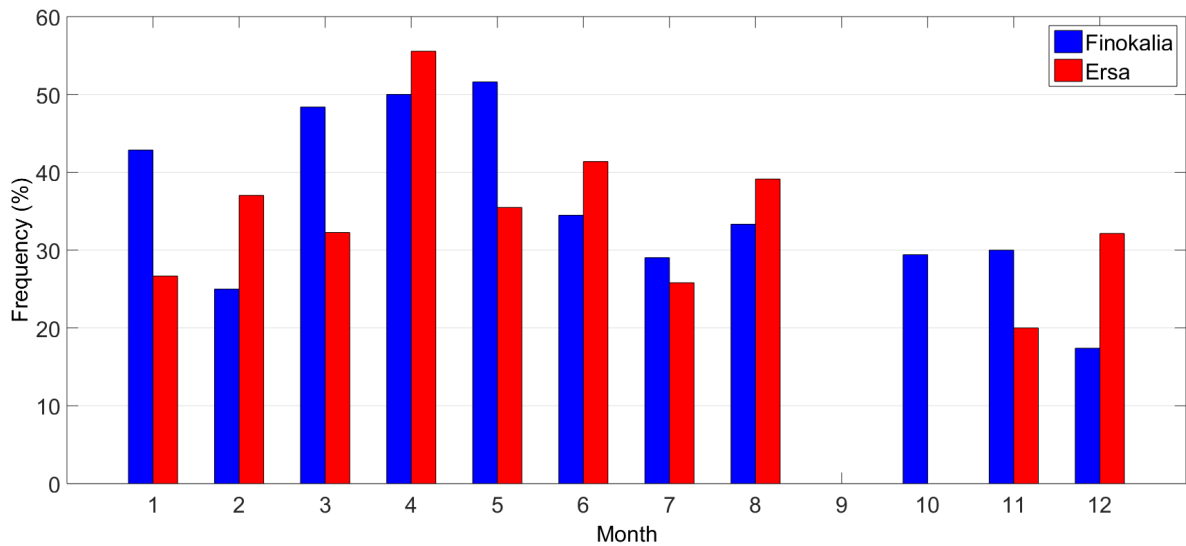
675   Figure 2: Monthly mean NPF frequencies at Finokalia and Ersa.
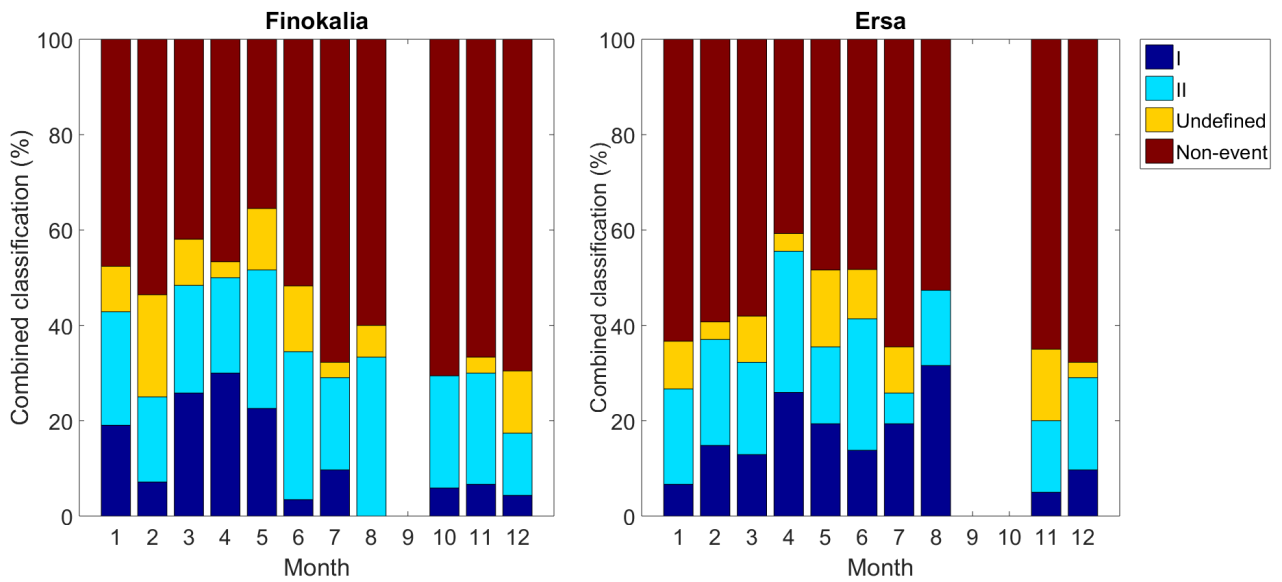
Figure 3: Monthly classification of the measurement days into event (I and II), undefined and non-event categories in Finokalia and Ersa.
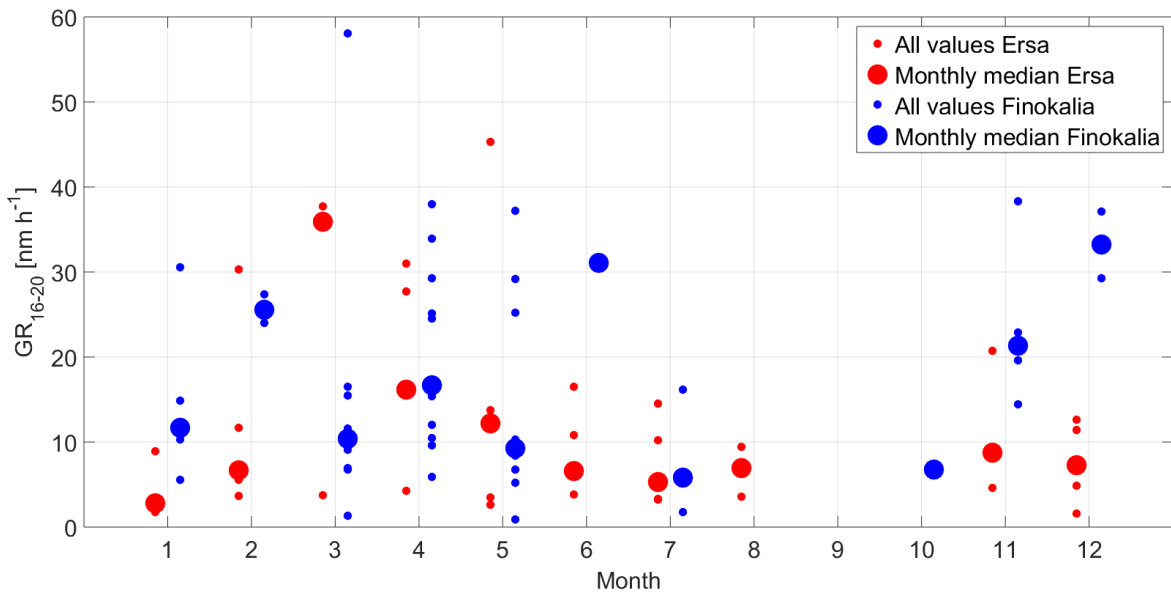
Figure 4: Annual variation of particle growth rate calculated for the range 16 – 20 nm at Ersa and for type I events. Small dots represent all values while large dots stand for median values.

686
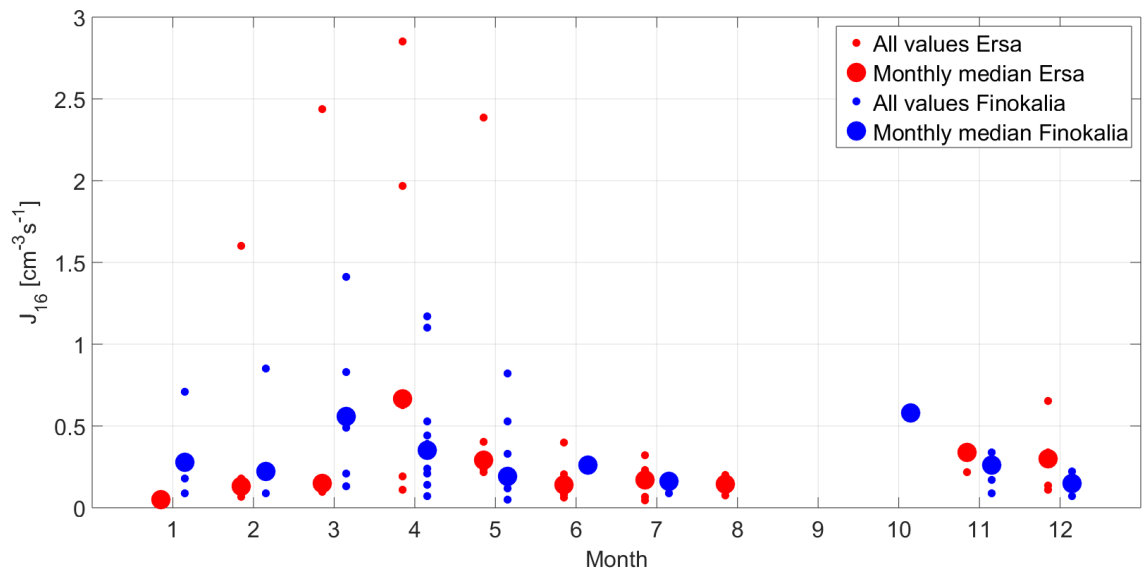
Figure 5: Annual variation of the 16 nm particle formation at Ersa and Finokalia for type I events. Small dots represent all values while large dots stand for median values.

690

691
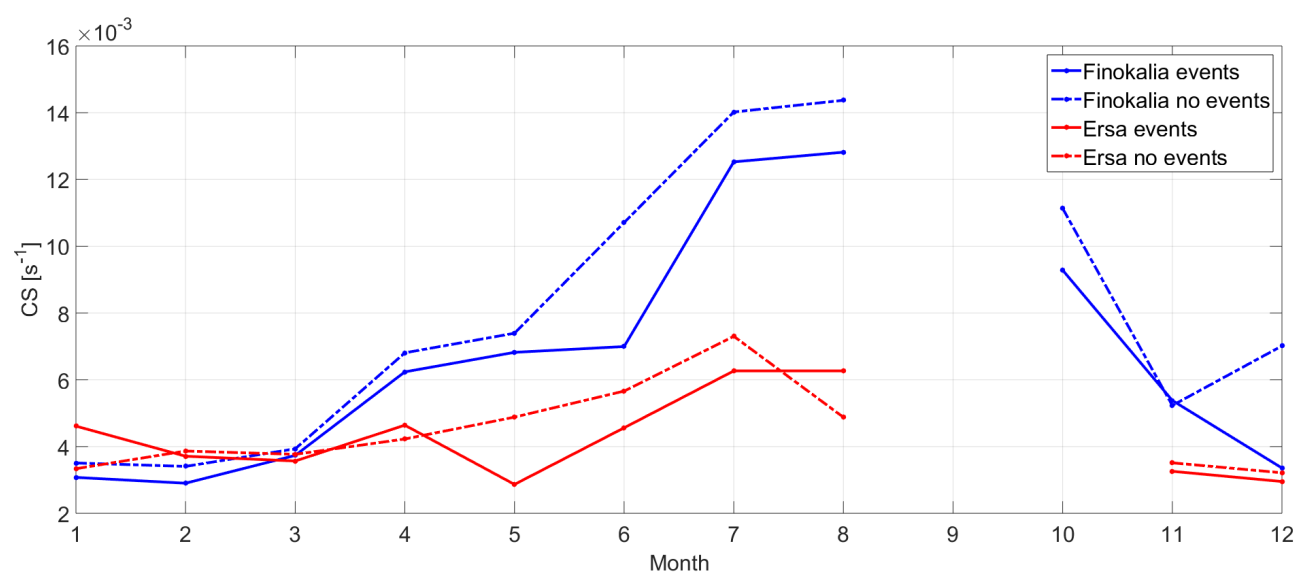
Figure 6: Median values of condensation sink (CS) reported separately for event and non-event days in Finokalia and Ersa.
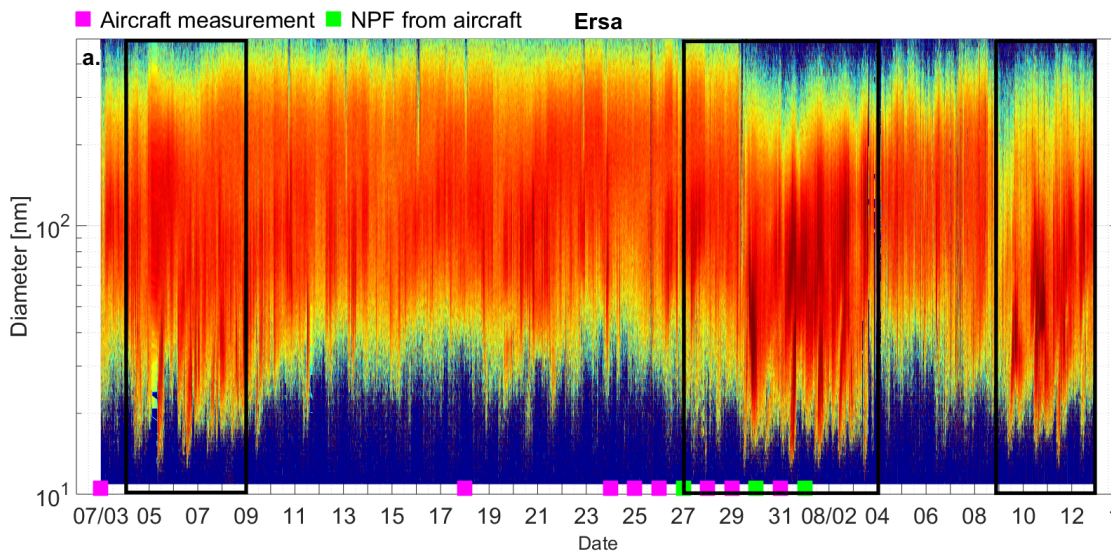
694
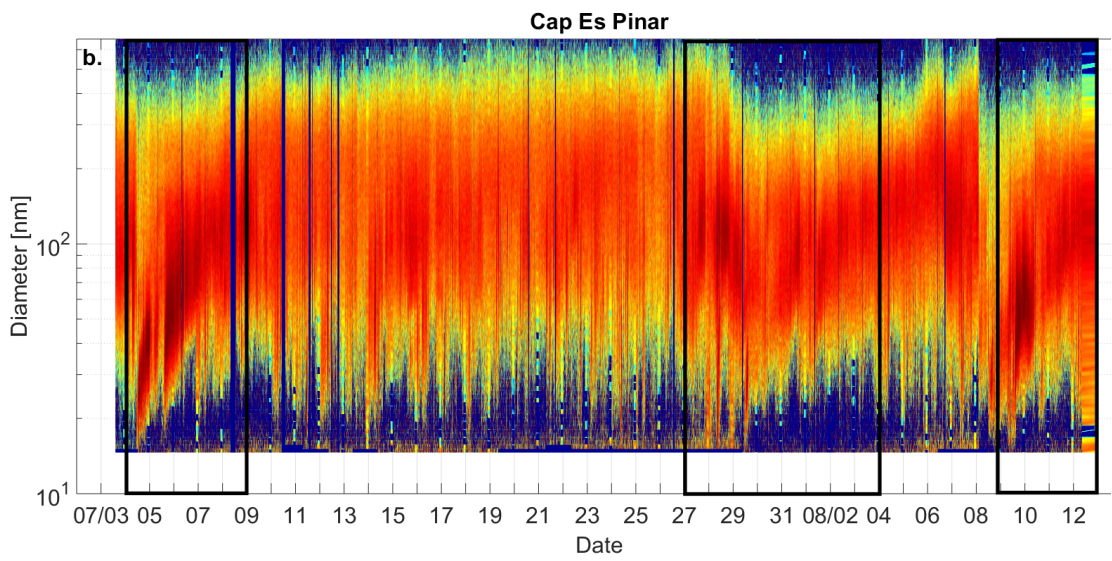
695
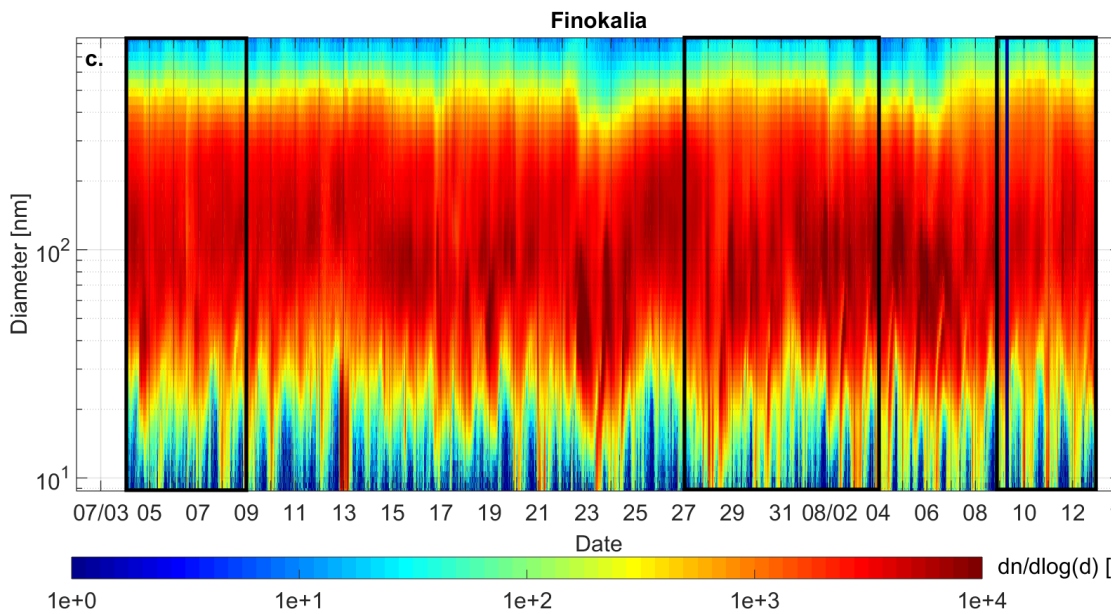
696

697   Figure 7: SMPS particle number size distribution in a. Ersa, b. Cap Es Pinar and c. Finokalia during
698   the SOP period. The three NPF episodes observed at large scale are highlighted on the spectra in the
699   black boxes. The days of occurrence of the ATR-42 flights are also shown, together with the detection
700   of NPF from these airborne measurements. Same color scale applies to a., b. and c..

701
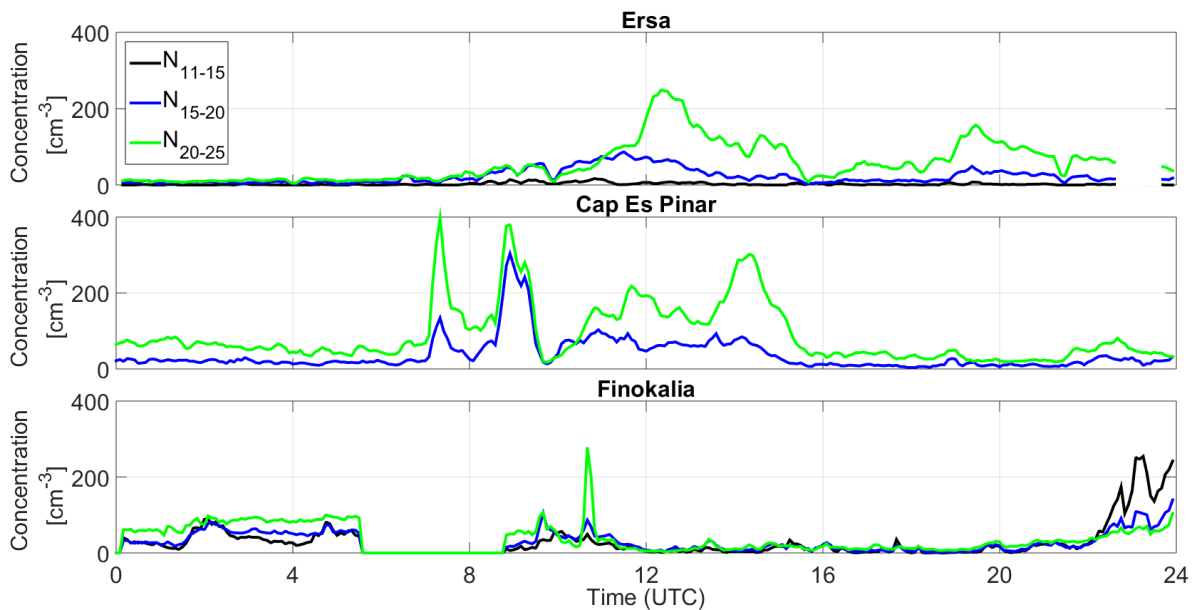
702   Figure 8: Temporal evolution of the particle concentrations in the size range 11-15 nm (black) (N_{11-15}),
703   15-20 nm (blue) (N_{15-20}) and 20-25 nm (green) (N_{20-25}) for August 9th event.

704
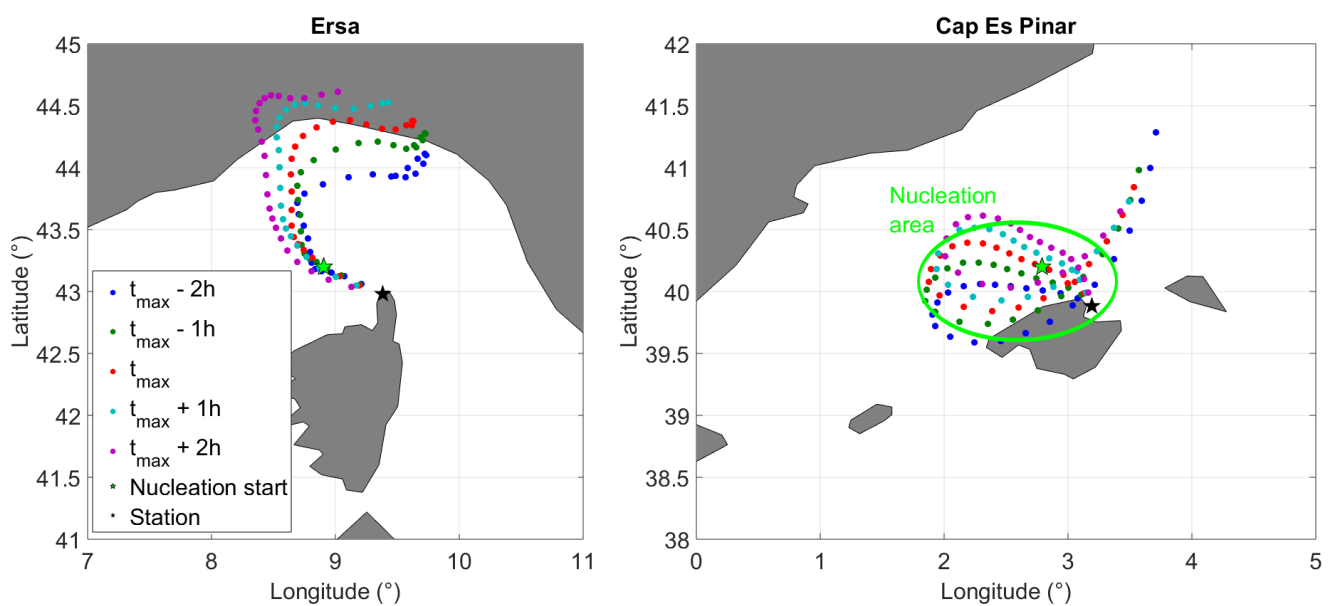
705

706   Figure 9: Back trajectories of air masses sampled in Ersa and Cap Es Pinar on August 9th at t_{max}, when
707   20 nm particles concentration is maximum, and during the two hours that precede and follow this

708 maximum. The location where nucleation initially occurs upstream the station is marked with a green
709 star.

710

712
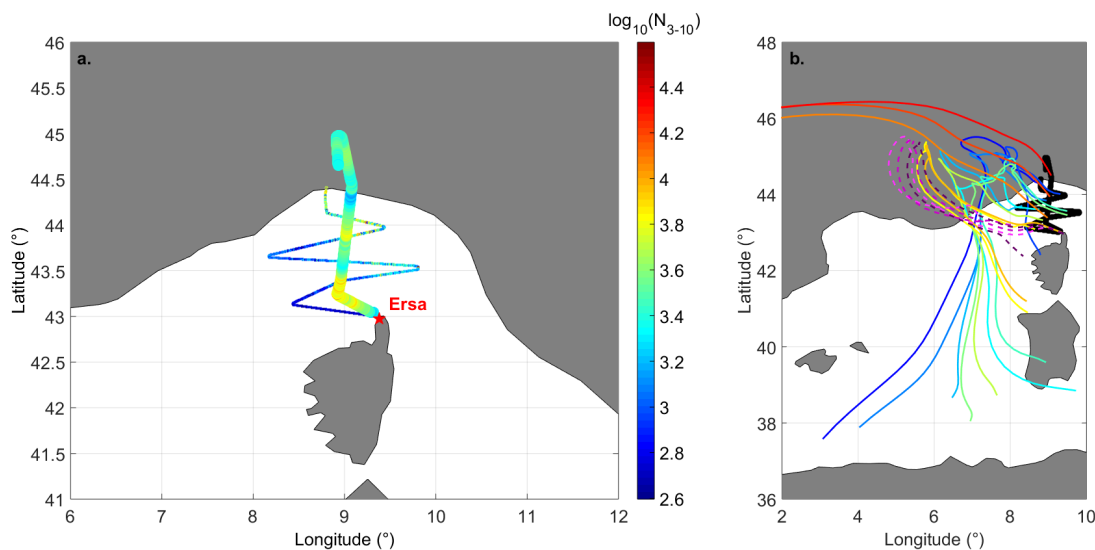
713

714 Figure 10: a. N_{3-10} above the threshold value along the flight path performed on July 30th. Large size
715 dots stand for high altitude measurements (~ 3400 m a.s.l.) while small size dots stand for low altitude
716 measurements (~ 215 m a.s.l.); b. Air mass back trajectories calculated along the flight path (black
717 line) every ten minutes (solid colored lines) together with the back trajectories of air masses arriving in
718 Ersa each hour during the same time period (dashed lines).

719
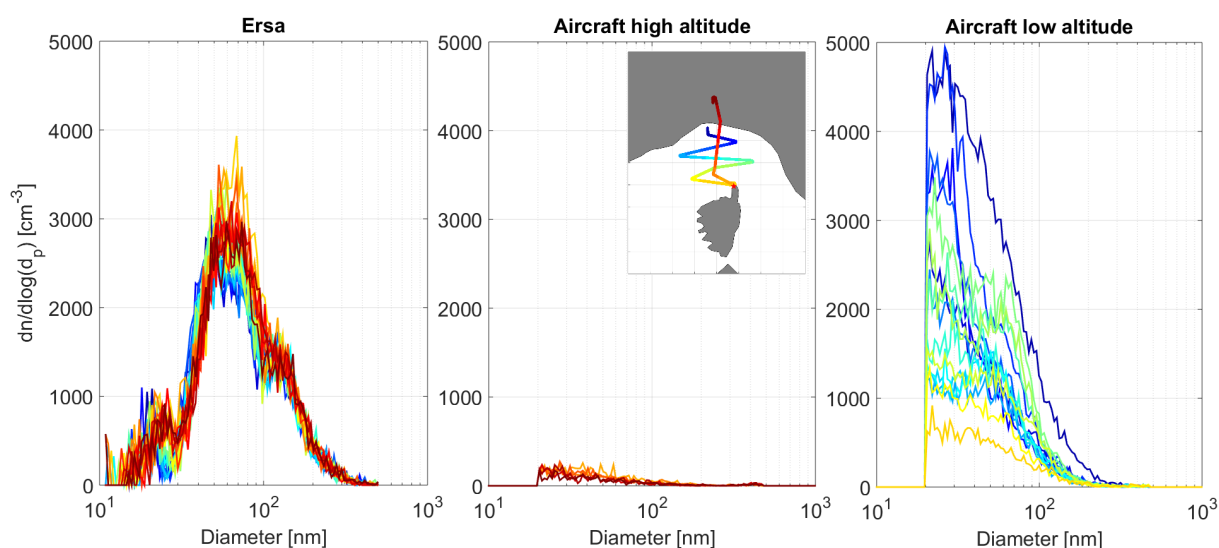
720

721 Figure 11: SMPS size distributions measured at Ersa (left panel) and onboard the ATR-42 at high
722 altitude (~ 3400 m a.s.l.) (middle panel) and low altitude (~ 215 m a.s.l.) (right panel) on July 30th. The
723 color coding of the size distributions corresponds to the location of the aircraft, as shown on the insert
724 of the middle panel.

725

726

728

729
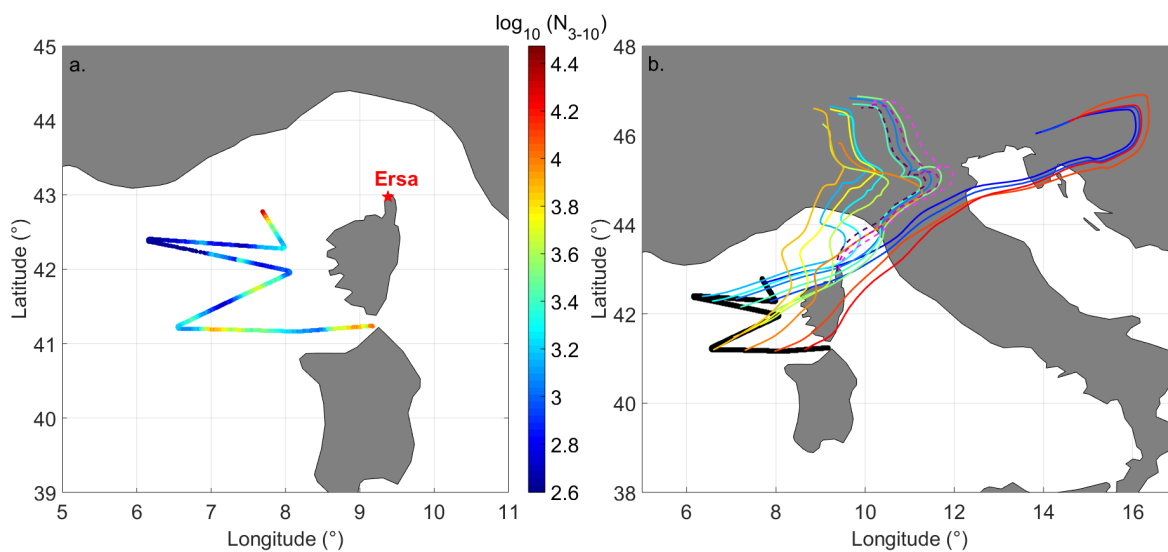
Figure 12: a. N_{3-10} above the threshold value along the flight path; b. Air mass back trajectories (solid lines) calculated along the flight path (black line) every ten minutes (solid colored lines) together with the back trajectories of air masses arriving in Ersa each hour during the same time period (dashed lines) during the August 1st flight.

734

735
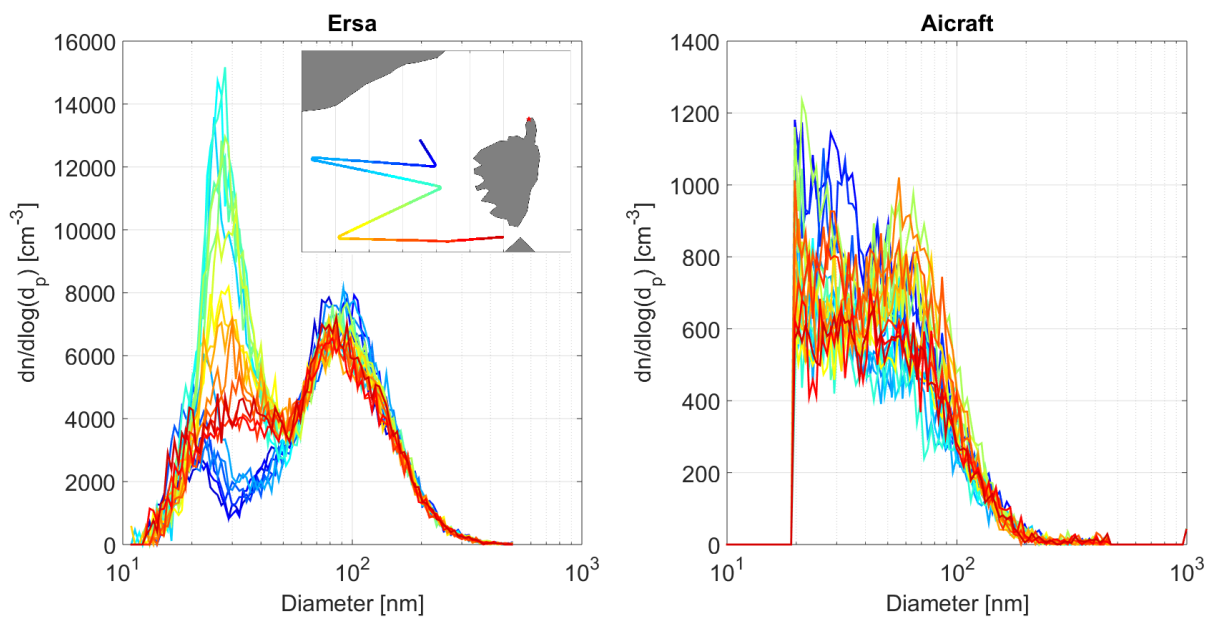
Figure 13: Ground based (left panel) and airborne (right panel) SMPS size distributions measured on August 1st . The color coding of the spectra corresponds to the location of the aircraft, as shown on the insert of the left panel.
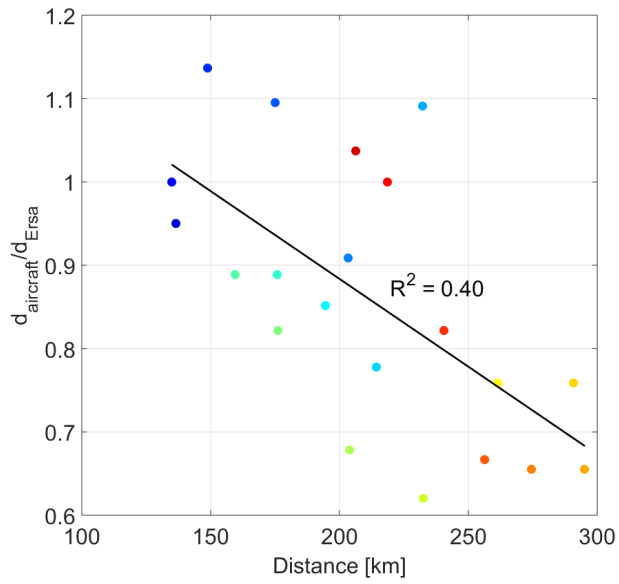
Figure 14: Ratio of nucleation mode diameters measured onboard the ATR-42 over that calculated in Ersa as a function of the distance between the aircraft and Ersa on August 1st. The color coding of this scatter plot matches with the location of the aircraft showed on the insert of the left panel of Figure 13.